Total Cavopulmonary Connection Flow With Functional Left Pulmonary Artery Stenosis: Angioplasty and Fenestration In Vitro

Kerem Pekkan, Hiroumi D. Kitajima, Diane de Zelicourt, Joseph M. Forbess, W. James Parks, Mark A. Fogel, Shiva Sharma, Kirk R. Kanter, David Frakes and Ajit P. Yoganathan

Circulation 2005;112;3264-3271; originally published online Nov 14, 2005;
DOI: 10.1161/CIRCULATIONAHA.104.530931
Circulation is published by the American Heart Association. 7272 Greenville Avenue, Dallas, TX 72514
 Print ISSN: 0009-7322. Online ISSN: 1524-4539

Total Cavopulmonary Connection Flow With Functional Left Pulmonary Artery Stenosis

Angioplasty and Fenestration In Vitro

Kerem Pekkan, PhD; Hiroumi D. Kitajima, MSc; Diane de Zelicourt, MSc; Joseph M. Forbess, MD; W. James Parks, MD; Mark A. Fogel, MD; Shiva Sharma, MD; Kirk R. Kanter, MD; David Frakes, PhD; Ajit P. Yoganathan, PhD

Background—In our multicenter study of the total cavopulmonary connection (TCPC), a cohort of patients with long-segment left pulmonary artery (LPA) stenosis was observed (35%). The clinically recognized detrimental effects of LPA stenosis motivated a computational fluid dynamic simulation study within 3-dimensional patient-specific and idealized TCPC pathways. The goal of this study was to quantify and evaluate the hemodynamic impact of LPA stenosis and to judge interventional strategies aimed at treating it.

Methods and Results—Simulations were conducted at equal vascular lung resistance, modeling both discrete stenosis (DS) and diffuse long-segment hypoplasia with varying degrees of obstruction (0% to 80%). Models having fenestrations of 2 to 6 mm and atrium pressures of 4 to 14 mm Hg were explored. A patient-specific, extracardiac TCPC with 85% DS was studied in its original configuration and after virtual surgery that dilated the LPA to 0% stenosis in the computer medium. Performance indices improved exponentially (R^2>0.99) with decreasing obstruction. Diffuse long-segment hypoplasia was ≈50% more severe with regard to lung perfusion and cardiac energy loss than DS. Virtual angioplasty performed on the 3-dimensional Fontan anatomy exhibiting an 85% DS stenosis produced a 61% increase in left lung perfusion and a 50% decrease in cardiac energy dissipation. After 4-mm fenestration, TCPC baffle pressure dropped by ≈10% and left lung perfusion decreased by ≈8% compared with the 80% DS case.

Conclusions—DS <60% and diffuse long-segment hypoplasia <40% could be considered tolerable because both resulted in only a 12% decrease in left lung perfusion. In contrast to angioplasty, a fenestration (right-to-left shunt) reduced TCPC pressure at the cost of decreased left and right lung perfusion. These results suggest that pre-Fontan computational fluid dynamic simulation may be valuable for determining both the hemodynamic significance of LPA stenosis and the potential benefits of intervention. **(*Circulation*. 2005;112:3264-3271.)**

Key Words: angioplasty ■ blood flow ■ Fontan procedure ■ stenosis ■ magnetic resonance imaging

Palliative surgical treatments[1,2] of the single ventricle heart defect result in diverse, complicated, and clinically critical morphologies. Among other factors, early deaths and poor outcomes are associated with high pulmonary vascular resistance and hypoplastic or distorted pulmonary arteries.[3] All stage 1 reconstructions and palliative initial shunt operations have the potential to obstruct branch pulmonary arteries, having both immediate effects on pulmonary function and long-term effects in the form of asymmetrical arterial growth and remodeling patterns.[4,5] Later stages of the total cavopulmonary connection (TCPC) surgery further complicate blood flow dynamics, affecting cardiac loading, lung perfusion, and hepatic blood distribution.[6–8] Stenotic lesions of the pulmonary arteries can contribute to significant downstream hypoplasia of pulmonary arteries, ventilation/perfusion mismatch, impaired postsurgery revascularization, thromboembolism, limited exercise capacity, increased atrial level shunting, atrial/ventricular arrhythmias, and protein-losing enteropathy, all important concerns during and after surgery and for the quality of postoperative life.[4,9,10]

Received December 20, 2004; revision received July 14, 2005; accepted August 26, 2005.

From the Cardiovascular Fluid Mechanics Laboratory, Wallace H. Coulter Department of Biomedical Engineering, Georgia Institute of Technology, Atlanta (K.P., H.D.K., D.d.Z., D.F., A.P.Y.); Division of Cardiothoracic Surgery, Department of Surgery, Emory University School of Medicine, Atlanta, Ga (J.M.F., K.R.K.); Department of Cardiology, Emory University School of Medicine, Sibley Heart Center Cardiology, Atlanta, Ga (W.J.P.); Division of Cardiology, Children's Hospital of Philadelphia, Philadelphia, Pa (M.A.F.); and Pediatric Cardiology Associates, Atlanta, Ga.

The online-only Data Supplement can be found with this article at http://circ.ahjournals.org/cgi/content/full/CIRCULATIONAHA.104.530931/DC1.

Presented in part at the American Heart Association 2004 Scientific Sessions, New Orleans, La, November 7–10, 2004, and published in abstract form (*Circulation.* 2004;110[suppl III]:III-737).

Correspondence to Ajit P. Yoganathan, PhD, The Wallace H. Coulter Distinguished Faculty Chair in Biomedical Engineering, Regents Professor, Associate Chair for Research, Wallace H. Coulter School of Biomedical Engineering, Georgia Institute of Technology and Emory University, Room 2119, U.A. Whitaker Bldg, 313 Ferst Dr, Atlanta, GA 30332–0535. E-mail ajit.yoganathan@bme.gatech.edu

Circulation **is available at http://www.circulationaha.org** **DOI: 10.1161/CIRCULATIONAHA.104.530931**

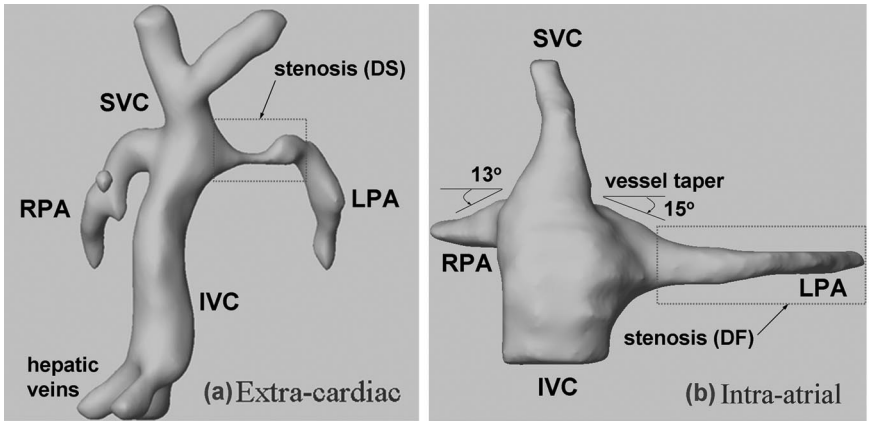

Figure 1. a, A 3D anatomic reconstruction of an extracardiac TCPC having DS-type LPA stenosis before the virtual intervention. Degree of stenosis is 85% in the CSA. b, Tapered pulmonary branches of an intra-atrial TCPC. This anatomy is provided as an example for a diffuse pulmonary stenosis (≈60% CSA) analyzed earlier.[21] The angle of vessel taper is based on the half-angle of the hydraulic cross-sectional diameter change. The extracardiac anatomy (a) features a half-diameter offset in the A-P direction.

Surgical patch augmentation of the left pulmonary artery (LPA),[11,12] balloon angioplasty, and fenestration[13] are common interventions used to overcome elevated Fontan baffle pressures and poor left lung perfusion, which are associated with stenotic pulmonary arteries. In this study, to compare the hemodynamic outcomes associated with these options, LPA augmentation and fenestration were performed virtually in a computer medium on idealized models and on a selected patient-specific extracardiac TCPC.

Fenestration has been demonstrated to yield lower systemic venous pressures and improved ventricle filling, cardiac output, and overall oxygen delivery.[14] Although some institutions advocate routine fenestration,[9] others argue that it should be used more selectively,[15] balancing the potential benefits against the risks and costs of an additional intervention for closure. A mathematical model, as presented here, that quantifies left and right lung perfusion, TCPC baffle pressure, the effects of different fenestration sizes, and atrial pressures would complement previous studies[9,14,15] and contribute to clinical understanding and interventional plans.

The importance of geometric features for long-term TCPC efficiency has been demonstrated through a series of numerical and experimental in vitro studies.[16–19] Recent anatomic fluid dynamic studies[20,21] of the TCPC have tried to identify the relative contribution of different features and the configuration of the central "+"-shaped connection site and the connecting inferior (IVC) and superior vena cava (SVC) and left and right pulmonary arteries (RPA) to the global flow field. Each of these components has characteristic morphological variations and an equal-order-of-magnitude significance to the overall hydrodynamic performance and pressure drop. The influence of different IVC configurations for a given Glenn stage anatomy is studied via computational fluid dynamic (CFD), and the benefits of specific anastomoses are demonstrated.[22] This article quantifies fluid dynamics effects of component-level morphological variations of the LPA outflow branch in idealized models and in patient-specific anatomies focused on stenotic LPA morphologies.

Methods

Cohort of TCPC With LPA Stenosis

A multicenter Fontan patient MRI database has been assembled to study the anatomic elements of the TCPC. Informed consent was obtained, and all associated studies were approved by the Internal Review boards of the Children's Hospital of Philadelphia, Children's Healthcare of Atlanta, University of North Carolina, and Georgia Institute of Technology. On examination of the MRI data and corresponding 3-dimensional (3D) TCPC reconstructions, a cohort (13 of 37 cases, 35%) exhibited LPA stenosis. Further analysis revealed that 10 of 13 patients with LPA stenosis (77%) carried the diagnosis of hypoplastic left heart syndrome in which the aorta is augmented with a patch of the larger main PA. The enlarged neo-aorta is observed to cause superior and anterior compression on the LPA, which is largely immobilized because of the left mainstream bronchus. A 3D anatomic reconstruction of a typical TCPC having discrete LPA stenosis is presented in Figure 1a.

Our database revealed 2 types of stenoses: Discrete stenosis (DS) or diffuse long-segment hypoplasia (DF). In DS (Figure 1a), the lesion is asymmetric about the vessel axis before distally returning to the proximal vessel diameter. A DF is characterized by a gradual taper, as shown in Figure 1b, in which the diameter does not return to its original caliber distal to the neo-aortic reconstruction. DF can also be associated with the mismatch between the native vessel and the proximal TCPC, producing a level of taper that can lessen as the native vessel grows if there is sufficient blood flow.

Computational Models

The TCPC models were analyzed with CFD techniques, providing detailed 3D flow fields, lung perfusions, pressure drops, and hydrodynamic power losses. The analysis requires creation of an idealized model geometry designed within a computer-aided design package or by reconstructing it from anatomic MRI patient data. The next step is grid generation in which the vessel volume is divided into thousands of smaller volumes or computational elements (grids or meshes). At each element, the governing conservation equations of mass and momentum for blood fluid flow are solved. Although there are no assumptions involved in the mathematical framework of blood flow, a credible numerical solution of the governing equations requires diligent boundary condition specification, global and local mesh verification studies, and in vitro experimental validation. Further references are provided in an earlier review.[20] Specific technical details of CFD validation and verification studies are provided in the Appendix (found in the online-only Data Supplement at http://circ.ahjournals.org/cgi/content/full/CIRCULATIONAHA.104.530931/DC1).

Idealized TCPC With DS and DF

In this study, idealized TCPC models with parametric dimensions are used to explore the effects of varying specific parameters such as degree of stenosis in the context of a well-understood idealized model. This process is analogous to altering a single variable (ie, scaled up or down in size) in a multivariable framework to investigate its impact on system performance.

The 1-diameter offset idealized TCPC model without stenosis, previously studied by Ensley et al,[18] was reproduced as the reference model (Figure 2a) with a reduction in cross-sectional area (CSA) of 0%. CFD calculations[23] and in vitro particle image velocimetry

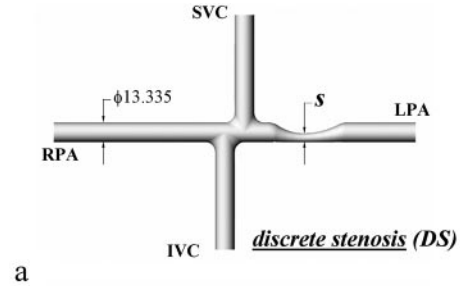

a

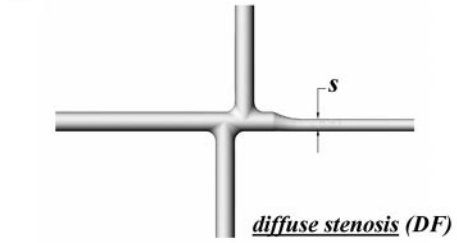

MODELS	% Area Reduction (CSA)	s (mm)
One Dia. Offset (Reference)	0	13.335
DS-1	20	11.9272
DS-2	40	10.3292
DS-3	60	8.4338
DS-4	80	5.9636
DF-1	20	11.9272
DF-2	40	10.3292
DF-3	60	8.4338
DF-4	80	5.9636

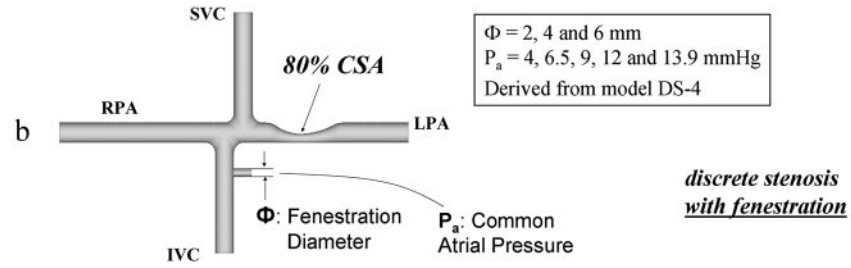

b

Figure 2. Idealized TCPC models with the geometric dimensions and configurations studied in CFD. a, DF and DS stenotic lesions. CSA reductions and the minimum LPA branch diameters are tabulated for these 9 idealized models. b, Idealized 80% CSA model with fenestration. The table lists the studied fenestration diameters and common atrial pressures.

experiments[24] on this reference configuration demonstrate low hydrodynamic power loss characteristics resulting from the stable buffer vortex located at the offset region.[18] Larger, surgically impractical offset distances have higher loss indices and can result in undesirable hepatic blood distribution. In this model, all venae cavae and pulmonary arteries were held constant at 13.335 mm, a dimension retained by Ensley et al[18] based on the chest MRI of an 8-year-old Fontan patient.[18]

Idealized models with various degrees of stenosis (0% to 80%) were created by introducing a smoothly varying obstruction into the functional LPA of the 1-dimensional offset reference model (Figure 2a). The 2 basic, anatomically observed, eccentric stenosis morphologies with convergent-divergent (DS) and convergent-only (DF) area variation were realized. The stenosis region, located 2.5 diameters distal from the SVC axis, had 1.5 and 2.0 diameters of convergent and divergent segments, respectively.

TCPC with Fenestration

The 1-dimensional offset idealized model having 80% stenosis in CSA (mean Fontan baffle pressure, 16 mm Hg) was modified to include a fenestrated communication between the pulmonary venous (common) atrium and the TCPC baffle (Figure 2b). Simulations were performed for 2- and 4-mm fenestrations, corresponding to the standard coronary bypass punches, and for a 6-mm opening, representing the upper-limit fenestration that may be used with an adjustable snare device.[25] Five pulmonary venous atrium pressure values (4, 6.5, 9, 12, and 13.9 mm Hg) were imposed at the outlet of the fenestration to span the relevant range of transpulmonary pressure gradients. The fenestration was located on the IVC 2 vessel diameters proximal from the PA axis.

Patient-Specific Anatomical TCPC

Reconstruction Methods and Geometry

Previous reconstruction of 3D patient-specific morphologies from MRI has enabled detailed and realistic flow analyses.[21] The anatomic models are obtained from patient MRI data by enhancing the out-of-plane image resolution with an adaptive control grid interpolation technique[26] and then segmenting the vessels of interest. The patient-specific TCPC fluid dynamic analysis methodology, which uses in vitro computational and experimental models, is described elsewhere.[20,27]

A typical extracardiac TCPC anatomy (Fontan Anatomy/Flow Database ID CHOP013) with a severe DS (85% CSA) was selected from our database[28] for analysis (Figure 1a). It featured hydraulic vessel diameters of 7.7, 8.8, 14.0, and 19.1 mm for the LPA, RPA, SVC, and IVC, respectively, and a smooth IVC baffle with uniformly constant diameter. Stenosis, where the hydraulic vessel diameter decreased to 3.0 mm, was located ≈15 mm (distal) from the IVC anastomoses.

Virtual Angioplasty

The 3D computational models allow modification, which mimics surgical alteration seen in vivo. Thus, the results of virtual surgery can be evaluated computationally. This approach was applied to an 85% LPA stenosis with virtual dilatation to 0%. No other part of the original connection geometry shown in Figure 1a was altered virtually.

Hydrodynamic Power Loss

The cardiac workload consumed in the TCPC to overcome flow resistance can be calculated (Equation A-1 in the Appendix). This power loss index represents both the pressure drop and global TCPC flow quality and has been established as a valid parameter for comparing the overall performance of different TCPC designs and surgical morphologies.[16–24] Furthermore, noninvasive clinical acquisition of this parameter in vivo is prospectively possible with cardiac phase-contrast MRI.[23]

Equal Vascular Lung Resistance Physiological Operating Point

Characteristics of TCPC models were obtained over a range of operating conditions by specifying varied LPA and RPA flow splits

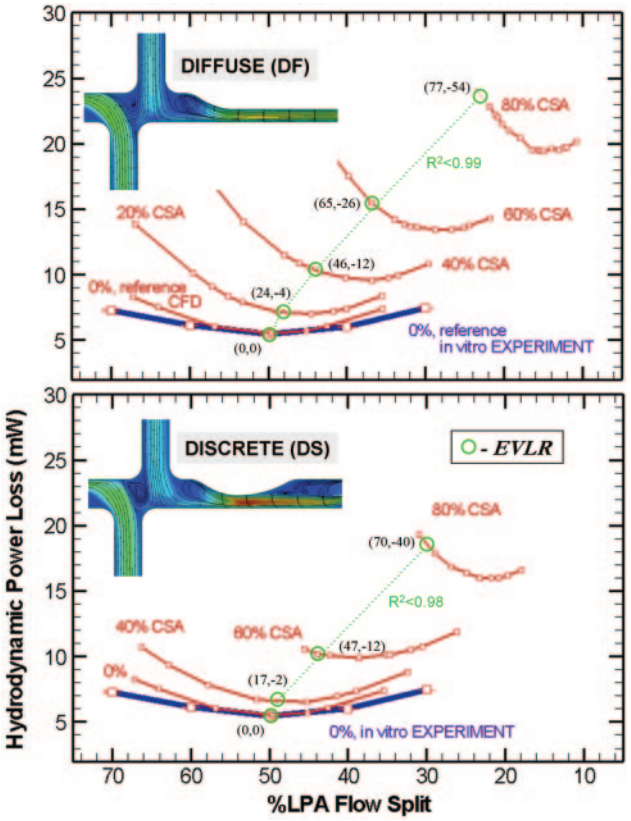

Figure 3. Left lung perfusion (percent of LPA flow split) vs hydrodynamic power loss for the DF and DS idealized models. EVLR operation points are indicated with circles. Red lines with small squares correspond to the CFD results at different LPA/RPA flow splits. CFD calculations are compared with the corresponding in vitro experimental results[18] for the 0% CSA reference model (dark blue curves with large squares and error bars of single SD). Values in parentheses as ordered pairs represent percent increase in cardiac power loss and decrease in left lung perfusion at EVLR with respect to the 0% CSA reference configuration. The least-squares-fit polynomial curve fitted to the computed EVLR points is plotted as green dotted line. R^2 values indicate good correlation. The small deviations are due mainly to the minor computational mesh differences between models. Velocity magnitudes (indicated by colors from red, 1.289 m/s, to blue, 0.086 m/s) and streamlines originated from IVC and SVC at the midcoronal plane for selected DS (DS-4) and DF (DF-4) stenosis models are plotted as insets corresponding to the EVLR states.

through a series of CFD simulations. Coupling these results with lumped parameter models of the pulmonary circulation enables comparison of different TCPC models or surgical alternatives in the same patient with known cardiac output, pulmonary vascular resistances, and IVC/SVC flow splits. Here, a vascular lung resistance of 1.8 Woods units was assumed for both lungs. This specific hemodynamic state is called the equal vascular lung resistance physiological operating point (EVLR) of the given TCPC.[21] Uneven vascular lung resistances may also be analyzed by specifying different values for each lung.

Results

Idealized Models

Discrete and Diffuse Stenosis

Figure 3 shows TCPC models with various degrees of DS and DF. Characteristic hydrodynamic power loss variations are plotted as a function of LPA flow split. For each model, the EVLR point is indicated. The EVLR operation point was observed to shift toward more balanced pulmonary flow splits as stenosis decreased, resulting in improved lung perfusion. Left lung perfusion increased and power loss decreased with decreasing stenosis severity (R^2>0.99). DF, a more severe condition than DS, resulted higher power losses and lower left lung perfusion, as shown in Figure 3. Good agreement between the computational results and in vitro experiments[18] for the zero-diameter offset reference model was also demonstrated.

Sample velocity magnitude distributions and flow streamlines along the midcoronal sections of the selected idealized TCPC models are plotted in Figure 3 at the EVLR conditions. For stenosis levels >40% CSA, disturbed flow patterns and recirculation regions were observed in the DS models. Branch TCPC pressures are tabulated with reference to the LPA pressure level in Table 1. The pressure values demonstrated a trend similar to that of the power losses. All pressure values were found to increase significantly with increasing degree of stenosis (0 to 5.2 mm Hg with reference to LPA outlet). TCPC pressures were 43±16% higher in the DF stenosis models compared with the DS models.

Improvements with Fenestration

For the 80% CSA idealized model (DS-4), the 4-mm fenestration decreased the TCPC baffle pressure by 8% to 14%, depending on the pulmonary venous (common) average atrial pressure. As illustrated in Table 2, elevated pulmonary venous atrium pressures diminished the effects of the fenestration as a result of a lower transfenestration gradient. As expected, larger fenestrations lead to improved pressures in the TCPC baffle. On the other hand, the shunt through the 4-mm fenestration worsened lung perfusion by 8% to 17% on the left and 11% to 15% on the right. Values are summarized in Table 2 for other fenestration sizes and pulmonary venous atrium pressures calculated at the EVLR operation points.

In Figure 4, the cardiac power loss characteristics of selected fenestration models are plotted as a function of LPA flow split. Despite the LPA/RPA flow split differences, lower pulmonary venous atrium pressures and larger fenestrations

TABLE 1. Branch Pressure Values for Idealized Models With No Fenestration

Models	Area Reduction (CSA), %	SVC Pressure, mm Hg	IVC Pressure, mm Hg	RPA Pressure, mm Hg
DS-1	20	0.7	0.6	0.0
DS-2	40	1.0	0.9	0.3
DS-3	60	1.7	1.6	0.8
DS-4	80	4.1	4.2	3.0
DF-1	20	1.0	0.9	0.3
DF-2	40	1.4	1.4	0.7
DF-3	60	2.6	2.6	1.8
DF-4	80	4.9	5.1	3.5

Calculated with reference to the LPA distal to the stenosis region. Total cardiac output, 4 L/min; IVC/SVC flow split, 60/40.

TABLE 2. DS of 80% CSA With Fenestration (Idealized Model)

Fenestration Size, mm	Common Venous Atrium Pressure, mm Hg	RPA Flow, %	LPA Flow, %	Fenestration Flow, %	Fenestration Jet, m/s	Q_P/Q_S	TCPC Pressure, mm Hg	Power Loss, mW
0	NA	70	30	0	0	1.0	17.6	18.6
4	4.0	59	23.6	17.4	0.92	0.83	15.2	28.0
4	6.5	59.5	24.8	15.7	0.83	0.84	15.3	22.5
4	9.0	60	26.3	13.7	0.73	0.86	15.6	18.9
4	12.0	62	27.5	10.5	0.56	0.9	15.9	12.5
4	13.9	63	28.9	8.1	0.43	0.92	16.2	14.1
2	6.5	65	29.3	5.7	1.21	0.94	16.6	17.4
2	9	66	30.0	4.0	0.85	0.96	16.6	15.9
6	6.5	51	15.1	33.9	0.80	0.66	14.0	30.4
6	9	53	17.7	29.3	0.69	0.71	14.4	19.8

For each model, calculated values correspond to the EVLR point. Percent flow distributions are based on the total cardiac output of 4 L/min. Q_P/Q_S indicates pulmonary-to-systemic flow ratio.

were found to increase the power loss and systemic-to-atrial shunt flow rate.

Patient-Specific Anatomical Models

Flow Fields

Pressure distribution along the TCPC pathway and flow streamlines are plotted in Figure 5 for the original extracardiac TCPC anatomy and the modified model without stenosis. Figure 5 shows that streamlines originating from the same locations in both models followed different paths. For the stenosis model, both IVC and SVC flows were preferentially directed to the right lung, whereas equal distribution was attained after stenosis dilatation. Swirling flow stream patterns, a common characteristic of the TCPC, were observed proximal to both branches, preferentially at the LPA.

Hemodynamic Improvements With Virtual Angioplasty

The hydrodynamic power loss characteristics were different for the 2 anatomies, as shown in Figure 6. The model with 85% CSA had very high energy loss, especially with increased LPA flow split. After LPA dilatation, the power loss curve was more symmetric with respect to the left/right flow split, causing the EVLR operating point to be much closer to an equal flow split. The virtual angioplasty operation resulted in notable performance improvements in left lung perfusion and hydrodynamic energy loss as 61% and 50%, respectively. The actual calculated values are labeled in Figure 5.

Discussion

Virtual LPA angioplasty offers a method to evaluate surgical options based on patient MRI. Morphing a patient anatomy to mimic changes made during surgery allows postoperative anatomy to be realized computationally without in vivo execution. Flow conditions within the anatomy can then be evaluated with the methods described here. The promise of virtual surgery and simulation is further supported by the results of flow studies in which a marked decrease in cardiac power loss over all pulmonary flow splits and increased lung perfusion was observed, as illustrated in Figure 5. In addition to providing a 3D sense of the intended procedure, this quantification of surgical benefits can offer information useful for evaluating different intervention strategies such as angioplasty and/or fenestration.

Large variations in patient anatomies make it difficult to characterize the TCPC as 1 generalized model. Our comparative patient-specific hemodynamic study is supported by an extensive set of simulations in idealized models, ≈500 individual CFD runs, which demonstrated the relative effects

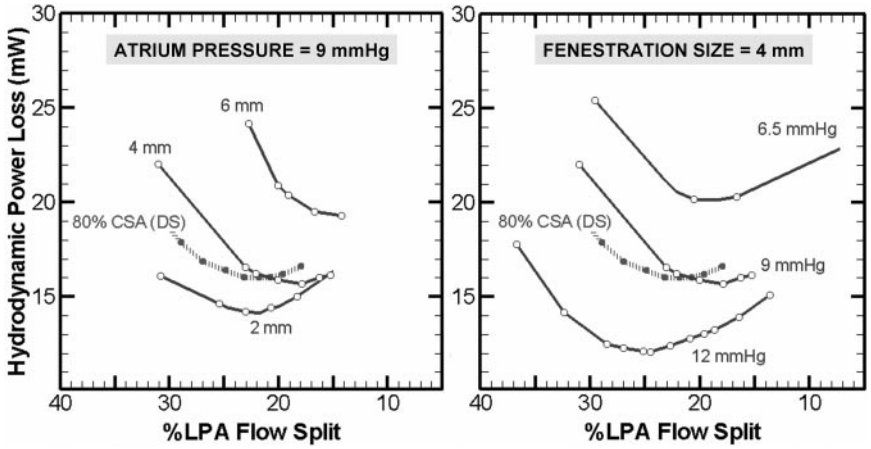

Figure 4. Hydrodynamic power loss with fenestration as a function of left lung perfusion (percent of LPA flow split) for the DS 80% CSA idealized model, DS-4, with different fenestration sizes (left) and atrium pressures (right). Corresponding EVLR operation points are tabulated in Table 1.

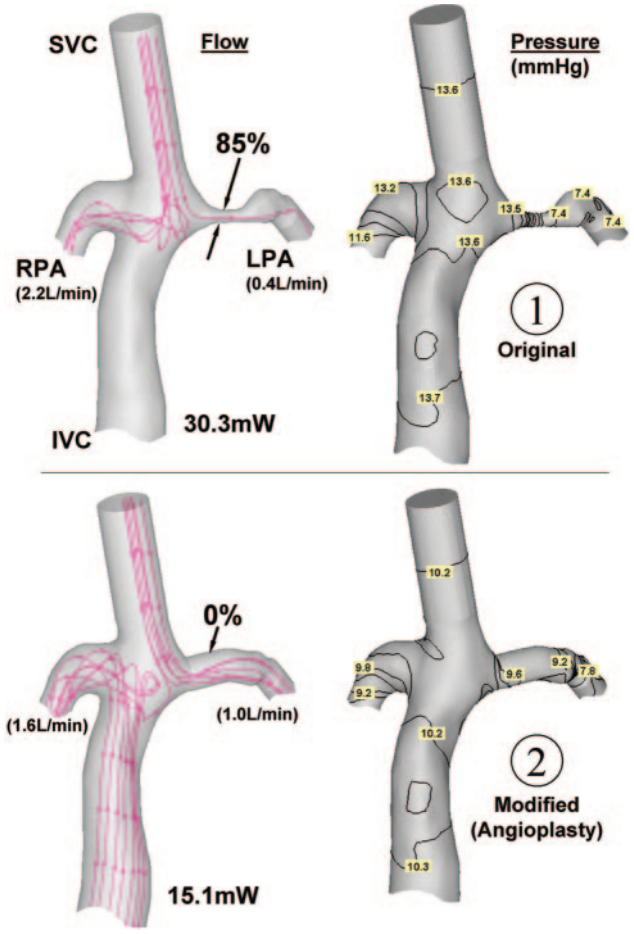

Figure 5. Computed flow streamlines showing the path followed by the incoming caval flow (left) and the TCPC pressure fields (in mm Hg) (right) are presented for the original anatomy with severe LPA stenosis (85% CSA), as shown on top and indicated with "1." Corresponding flow streamlines and pressure are shown on bottom for the modified anatomy in which the stenosis is dilated to 0° in the computer, as indicated with "2." For both anatomic models, calculated lung perfusions and cardiac energy losses are labeled for comparison. Streamlines are originated from the identical locations. For the original model, only the SVC streamlines are plotted to clearly show the biased SVC flow distribution resulting from stenosis.

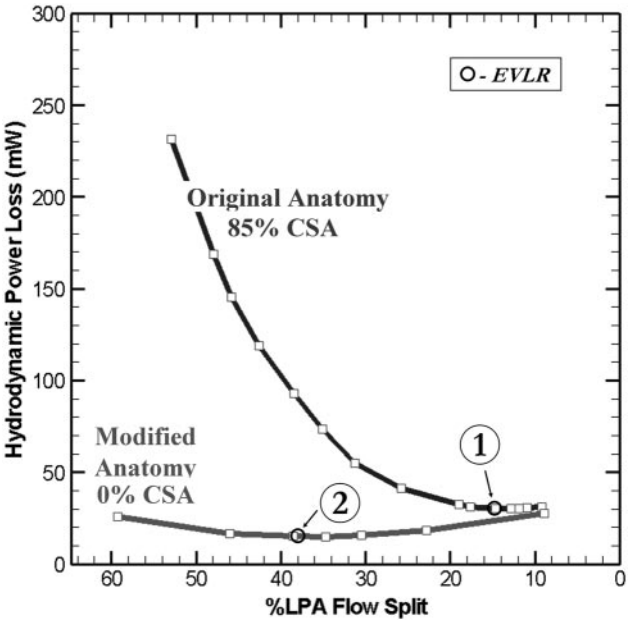

Figure 6. Hydrodynamic power losses vs LPA flow split of the original anatomy (1), severe LPA stenosis (85% CSA), and the modified anatomy (2) in which the stenosis is dilated to 0° in the computer. EVLR operating points are indicated for each model with green circles. All data represented in this plot were obtained from CFD. CFD solutions for these EVLR points are shown in Figure 5.

of dimensional variations on fluid dynamic performance. For any LPA stenosis or otherwise inefficient TCPC, the pressure in the baffle is seen to increase. The pressure loss in a DS would recover to a certain extent, whereas the pressure loss does not recover in DF, causing higher pressures within the baffle. Furthermore, a DS has the potential to cause significant distal flow disturbance and separation.

Power loss and perfusion results showed similarities for the idealized and anatomic 80% CSA DS models. This resulted from balanced effects of pulmonary branch size and cardiac output in these models (nominal branch PA diameter of the anatomic model is almost half of the idealized model, whereas the total cardiac output is ≈2 times higher). Our experience has shown that anatomic morphology and flow should be used when available for exact quantitative assessments. Idealized models are usually designed to study a single feature of the anatomy such as stenosis, fenestration, caval offset, or PA curvature; in the actual patient-specific morphologies, the results of all geometrical features are observed in a combined way. However, the idealized model studies are essential for understanding, and they provide a comparative "know-how" or "lookup table" when advanced CFD techniques are not readily available.

These results enabled a comparison between the effect of zero-offset and stenosis severity. We have studied a zero-offset model in our earlier work, which showed that a 1-dimensional offset, which is the reference model used here, reduces the hydrodynamic loss by ≈50%. Therefore, in the context of an idealized model at 4L/min cardiac output, flow resistance created as a result of a DS stenosis of 60% CSA is equivalent to having a zero offset in the TCPC. Both models yield approximately the same power losses but do not result in the same lung perfusion because the zero-offset model should yield a 50/50 EVLR and stenosis skews the EVLR toward the nonstenotic branch.

Fenestrations at the IVC simultaneously reduced the LPA and RPA flow. This is similar to operating the TCPC at a lower cardiac output and reduces the power loss in the TCPC as long as the transfenestration pressure gradient is low. Higher gradients cause increased losses because of very high flow through the fenestration. Flow through the fenestration can be unsteady, depending on the pressure variation in the atrium and baffle flow changes over the cardiac cycle. Although flow pulsatility (unsteady effects) was not studied here, simulations with a number of quasi-steady pressure levels as used here can picture these effects grossly. Variations in the fenestration location may warrant further investigation, even though only a slight effect on the hydrodynam-

ics is anticipated as long as the location remains on the IVC branch. Benefits of the reduced TCPC baffle pressure must be judged with regard to the corresponding reduction in lung perfusion. Based on the fluid dynamic factors alone, a cautious use of fenestrations or smaller diameters should be considered for patients with severely stenosed arteries and already poor left lung perfusion indices.

In current practice, the decision to intervene with LPA angioplasty rarely poses a question for DS; however, DF is more challenging. If amenable to intervention, highly stenosed morphologies are generally always addressed regardless of fenestration. The question of whether it is always necessary remains: Does the systematic intervention in these cases always lead to beneficial fluid dynamics and improved outcomes? The tools presented here offer a framework for elucidating this point. Our results showed that when applied individually, fenestration and angioplasty decrease the systemic venous pressure postoperatively by ≈3 mm Hg (≈20%) at moderate cardiac outputs. Angioplasty or stent placement involves risk and cost for the patient. Development of the proposed methodology to a dependable clinical level could prospectively identify cases in which intervention may not be necessary and the corresponding risk and cost are unwarranted.

In some cases, pediatric surgical decisions are based on "availability" or "necessity." For example, fenestrations are usually created through the use of a standard adult coronary artery punch of fixed diameter. This arbitrary size is used without consideration of fluid dynamics but in practice generally works well. However, the benefits of using varied punch sizes are unexplored. Without quantitative studies, it is unknown whether a 5-mm punch would result in better hemodynamics and clinical outcome than a 2-mm punch. Furthermore, given the current clinical understanding, it is unknown to what degree the left and right lungs will be perfused for a given TCPC anatomy and fenestration size or how large a systemic venous pressure drop will be created. The quantitative methods demonstrated here provide hemodynamic founding for answering these difficult questions. This information should be especially valuable for patients with preoperative instability in whom prolonged bypass time may be detrimental and operating time crucial. Verification of this approach, to quantify and demonstrate dynamic stability, is feasible and likely to be beneficial for the patient.

A large number of cases need to be explored to establish the efficacy of this approach and to identify areas of study and problem. This is a long-term strategy that needs to be developed and explored. Preintervention noninvasive and virtual techniques place within reach the ability to avoid pitfalls and achieve optimal surgical outcomes.

Conclusions

This study quantified the possible improvements in TCPC hemodynamics brought forth by performing a virtual angioplasty operation on a stenotic LPA. An actual anatomic extracardiac TCPC with severe stenosis was selected to illustrate the applicability of the CFD technique. MRI anatomical reconstructions and the preceding MRI data acquisition methodology are integrated to the fluid dynamics analysis, which could enable preinterventional outcome assessment for improved patient care. The anatomic case study is supported with parametric computational simulations in idealized models with 2 common stenosis types. It was found that for the same LPA diameter, DF is a more problematic condition than DS. Results for the anatomic TCPC before and after the virtual angioplasty operation should be referred to when available, and the idealized models should serve as comparative data when the detailed patient specific simulations are not available.

Fenestration and angioplasty were found to be equally effective in reducing high TCPC baffle pressures resulting from increased degrees of LPA stenosis. For all fenestrations studied, however, both the left and right lung perfusions were reduced as a result of the systemic venous-to-common atrial shunt. This correlates well with the clinical observation that for patients with less-than-ideal pulmonary artery anatomies, fenestration lowers Fontan baffle pressure to less morbid levels while resulting in lower systemic arterial oxygen saturation.

This study presents the first in a long line of detailed investigations. Advanced analysis techniques could potentially be useful in the clinical evaluation of complex patient hemodynamics and anatomies. Once more experience is gained with this type of analysis and with advances in hardware and software development in the years to come, these methodologies have the potential to be clinically acceptable and useful in surgical and clinical patient management. Most importantly, assessment of the predictive value of CFD simulation in clinical practice requires prospective testing in Fontan patients before and after intervention.

Acknowledgment

This work was supported by grant HL67622 from the National Heart, Lung and Blood Institute.

References

1. de Leval M, Kilner P, Gewillig M, Bull C. Total cavopulmonary connection: a logical alternative to atriopulmonary connection for complex Fontan operations: experimental studies and early experiences. *J Thorac Surg*. 1988;96:682–695.
2. McGuirk SP, Winlaw DS, Langley SM, Stumper OP, de Giovanni JV, Wright JG, Brawn WJ, Barron DJ. The impact of ventricular morphology on midterm outcome following completion total cavopulmonary connection. *Eur J Cardiothorac Surg*. 2003;24:37–46.
3. Goff DA, Blume ED, Gauvreau K, Mayer JE, Lock JE, Jenkins KJ. Clinical outcome of fenestrated Fontan patients after closure: the first 10 years. *Circulation*. 2000;102:2094–2099.
4. Agnoletti G, Boudjemline Y, Bonnet D, Sidi D, Vouhe P. Surgical reconstruction of occluded pulmonary arteries in patients with congenital heart defect: effects on pulmonary artery growth. *Circulation*. 2004;109:2314–2318.
5. Weber HS, Myers JL. Association of asymmetric pulmonary artery growth following palliative surgery for hypoplastic left heart syndrome with ductal coarctation, neoaortic arch compression, and shunt-induced pulmonary artery stenosis. *Am J Cardiol*. 2003;91:1503–1506.
6. Seliem MA, Murphy J, Vetter J, Heyman S, Norwood W. Lung perfusion patterns after bidirectional cavopulmonary anastomosis (hemi-Fontan procedure). *Pediatr Cardiol*. 1997;18:191–196.
7. Fogel MA, Weinberg PM, Chin AJ, Fellows KE, Hoffman EA. Late ventricular geometry and performance changes of functional single ventricle throughout staged Fontan reconstruction assessed by magnetic resonance imaging. *J Am Coll Cardiol*. 1996;28:212–221.
8. Hjortdal VE, Emmertsen K, Stenbøg E, Frund T, Schmidt MR, Kromann O, Sorensen K, Pedersen EM. Effects of exercise and respiration on blood

flow in total cavopulmonary connection. *Circulation*. 2003;108: 1227–1231.
9. Cochrane AD, Brizard CP, Penny DJ, Johansson S, Comas JV, Malm T, Karl TR. Management of the univentricular connection: are we improving? *Eur J Cardiothorac Surg*. 1997;12:107–115.
10. Srivastava D, Preminger T, Lock JE, Mandell V, Keane JF, Mayer JE Jr, Kozakewich H, Spevak PJ. Hepatic venous blood and the development of pulmonary arteriovenous malformations in congenital heart disease. *Circulation*. 1995;92:1217–1222.
11. Trant CA, O'Laughlin MP, Ungerleider RM, Garson A Jr. Cost-effectiveness analysis of stents, balloon angioplasty and surgery for the treatment of branch pulmonary artery stenosis. *Pediatr Cardiol*. 1997;18: 339–344.
12. Zahn EM, Dobrolet NC, Nykanen DG, Ojito J, Hannan RL, Burke RP. Interventional catheterization performed in the early postoperative period after congenital heart surgery in children. *J Am Coll Cardol*. 2004;43: 1264–1269.
13. Bridges ND, Lock JE, Mayer JE, Burnett J, Castaneda AR. Cardiac catheterization and test occlusion of the interatrial communication after the fenestrated Fontan operation. *J Am Coll Cardiol*. 1995;25:1712–1717.
14. Mavroudis C, Zales VR, Backer CL, Muster AJ, Latson LA. Fenestrated Fontan with delayed catheter closure: effects of volume loading and baffle fenestration on cardiac index and oxygen delivery. *Circulation*. 1992;86(suppl II):II-85–II-92.
15. Thompson LD, Petrossian E, McElhinney DB, Abrikosova NA, Moore P, Reddy VM, Hanley FL. Is it necessary to routinely fenestrate an extracardiac Fontan? *J Am Coll Cardiol*. 1999;34:539–544.
16. Sharma S, Goudy S, Walker P, Panchal S, Ensley A, Kanter K, Tam V, Fyfe D, Yoganathan A. In vitro flow experiments for determination of optimal geometry of total cavopulmonary connection for surgical repair of children with functional single ventricle. *J. Am. Coll. Cardiol*. 1996; 27:1264–1269.
17. de Leval M, Kilner P, Gewillig M, Bull C. Total cavopulmonary connection: a logical alternative to atriopulmonary connection for complex Fontan operations: experimental studies and early experiences. *J Thorac Surg*. 1988;96:682–695.
18. Ensley A, Lynch P, Chatzimavroudis GP, Lucas C, Sharma S, Yoganathan AP. Toward designing the optimal total cavopulmonary connection: an in vitro study. *Ann Thorac Surg*. 1999;68:1384–1390.
19. Lardo AC, Webber SA, Friehs I, del Nido PJ, Cape EG. Fluid dynamic comparison of intra-atrial and extracardiac total cavopulmonary connection. *J Thorac Cardiovasc Surg*. 1999;117:697–704.
20. Pekkan K, de Zélicourt D, Ge L, Sotiropoulos F, Frakes D, Fogel MA, Yoganathan AP. Physics driven CFD modeling of complex anatomical cardiovascular flows: a TCPC case study. *Ann Biomed Eng*. 2005;33: 284–300.
21. de Zélicourt D, Pekkan K, Wills L, Kanter K, Forbess J, Sharma S, Fogel M, Yoganathan AP. In vitro flow analysis of a patient specific intra-atrial TCPC. *Ann Thorac Surg*. 2005;79:2094–2102.
22. Migliavacca F, Dubini G, Bove EL, de Leval MR. Computational fluid dynamics simulations in realistic 3-D geometries of the total cavopulmonary anastomosis: the influence of the inferior caval anastomosis. *J Biomech Eng*. 2003;125:805–813.
23. Ryu K, Healy TM, Ensley AE, Sharma S, Lucas C, Yoganathan AP. Importance of accurate geometry in study of the total cavopulmonary connection: computational simulations and in vitro experiments. *Ann Biomed Eng*. 2001;29:844–853.
24. Ensley AE, Ramuzat A, Healy TM, Chatzimavroudis GP, Lucas C, Sharma S, Pettigrew R, Yoganathan AP. Fluid mechanic assessment of the total cavopulmonary connection using magnetic resonance phase velocity mapping and digital particle image velocimetry. *Ann Biomed Eng*. 2000;28:1172–1183.
25. Haas GS, Hess H, Black M, Onnasch J, Mohr FW, van Son JA. Extracardiac conduit Fontan procedure: early and intermediate results. *Eur J Cardiothorac Surg*. 2000;17:648–654.
26. Frakes D, Conrad C, Healy T, Monaco JW, Fogel M, Sharma S, Smith MJ, Yoganathan AP. Application of an adaptive control grid interpolation technique to morphological vascular reconstruction. *IEEE Trans Biomed Eng*. 2003;50:197–206.
27. de Zelicourt D, Pekkan K, Kitajima H, Frakes D, Yoganathan AP. Single-step transparent stereolithography of complex anatomical models for optical flow measurements. *J Biomech Eng*. 2005;127:204–207.
28. The Fontan project. Available at: http://fontan.bme.gatech.edu. Accessed on September 15, 2005.